



Cite this: *Nanoscale*, 2015, 7, 9655

Magnetically responsive star-block copolymeric micelles for controlled drug delivery and enhanced thermo-chemotherapy

Li Deng,^a Jie Ren,^{*a,b,c} Jianbo Li,^{*a,b} Junzhao Leng,^a Yang Qu,^a Chao Lin^c and Donglu Shi^{c,d}

Magnetically responsive drug-loaded micelles were designed and prepared for cancer therapy. These specially designed micelles are composed of the thermo-responsive star-block copolymer poly(ϵ -caprolactone)-*block*-poly(2-(2-methoxyethoxy)ethyl methacrylate-*co*-oligo(ethylene glycol)methacrylate) and Mn, Zn doped ferrite magnetic nanoparticles (MZF-MNPs). The thermo-responses of 6sPCL-*b*-P(MEO₂MA-*co*-OEGMA) copolymers were shown to be dependent on the MEO₂MA to OEGMA ratio. The lower critical solution temperature (LCST) of the star-block copolymers was controlled at 43 °C by adjusting the feed molar ratios of MEO₂MA/OEGMA at 92 : 8. With the anti-tumor drug doxorubicin (DOX) self-assembling into the carrier system, the thermo-responsive micelles exhibited excellent temperature-triggered drug release behavior. *In vitro* cytotoxicity results showed high biocompatibility of the polymer micelles. Efficient cellular proliferation inhibition by the drug-loaded micelles was found on the HepG2 cells under different treatments. The thermo-responsive polymer micelles are promising for controlled drug delivery in tumor therapy under an alternating magnetic field.

Received 28th January 2015

Accepted 20th April 2015

DOI: 10.1039/c5nr00642b

www.rsc.org/nanoscale

1. Introduction

Chemotherapy has been commonly used in cancer therapy.^{1–5} However, its low efficiency and high side effects have been a major concern. More recently, combining chemotherapy with hyperthermia has shown a significant improvement in tumor treatment. It was reported that drug cytotoxicity was improved by hyperthermia in chemotherapy through reinforced permeability of the tumor vasculature.^{6–9} The traditional thermo-chemotherapy relies primarily on whole-body or local hyperthermia, which leads to low synchronism in drug delivery.^{10–14} The synergistic effects of hyperthermia and chemotherapy need to be optimized on the tumor site. To address this critical issue, multifunctional thermo-responsive drug carriers have been designed and developed, utilizing the

temperature-sensitive copolymers and magnetic nanoparticles (MNPs) with the magnetothermal effect.^{15,16} Both the sensitivity and delivery efficiency can be enhanced by optimizing the lower critical solution temperature (LCST) of the temperature-sensitive polymer and the hyperthermia temperature of MNPs containing the chemotherapeutic agent.

Self-assembled copolymer nanoparticles have shown tremendous potential as chemotherapeutic drug-carriers.^{17–19} As a new temperature-sensitive copolymer, poly(2-(2-methoxyethoxy)ethyl methacrylate-*co*-oligo(ethylene glycol)methacrylate) (P(MEO₂MA-*co*-OEGMA)) was reported for its well-controlled LCST compared to the traditional temperature-sensitive copolymers, such as poly(*N*-isopropylacrylamide) (PNIPAM), which can be structurally modified by adjusting the ratio of co-monomers.^{20,21} P(MEO₂MA-*co*-OEGMA) also exhibits excellent biocompatibility, a crucial property in medical therapy.

As a promising tumor treatment, magnetic fluid hyperthermia has been introduced for targeted heating in an alternating magnetic field (AMF).^{22–25} Furthermore, the magnetic fluid can be used as the contrast agent in magnetic resonance imaging,²⁶ therefore it is versatile in both diagnosis and treatment of cancer.^{27–29} Compared with the most commonly used superparamagnetic iron oxide nanoparticles (SPIOs), many metal-doped spinel ferrites (MFe₂O₄, M=Mn, Ni, Co, etc.) exhibit a higher saturated magnetization (M_s) and stronger MRI contrast effect in the T2-weighted images owing to the

^aInstitute of Nano and Biopolymeric Materials, School of Materials Science and Engineering, Tongji University, 4800 Caoan Road, Shanghai 201804, China. E-mail: renjie6598@163.com; Fax: +86-21-69580234; Tel: +86-21-69580234

^bKey Laboratory of Advanced Civil Engineering Materials (Tongji University), Ministry of Education, Shanghai 201804, China. E-mail: lijianbo@tongji.edu.cn; Fax: +86-21-33515906; Tel: +86-21-33515906

^cShanghai East Hospital, The Institute for Biomedical Engineering and Nano Science, Tongji University School of Medicine, 150 Jimo Road, Shanghai 200120, China

^dThe Materials Science and Engineering Program, Department of Mechanical and Materials Engineering, College of Engineering & Applied Science, University of Cincinnati, Cincinnati, OH 45221-0012, USA

magneto-crystalline anisotropy.^{30,31} Meanwhile, a high specific absorption rate (SAR) is essential to the magnetic fluid for a better self-heating effect with a small amount of MNPs. Manganese and zinc doped ferrite (MZF, $Mn_xZn_{1-x}Fe_2O_4$) nanoparticles had been reported to exhibit higher SAR than other MFe_2O_4 .^{31,32}

In this study, magnetothermally responsive micelles were designed and prepared for cancer therapy. They were self-assembled from the temperature-sensitive star-block copolymers composed of hydrophobic poly(ϵ -caprolactone) (PCL) and hydrophilic P(MEO₂MA-co-OEGMA). Manganese and zinc doped ferrite (MZF, $Mn_xZn_{1-x}Fe_2O_4$) magnetic nanoparticles were encapsulated in the carrier system for magnetic hyperthermia heating. The LCST of micelles was accurately controlled by adjusting the ratio of MEO₂MA to OEGMA, and optimized at 43 °C. The magnetothermally responsive micelles loaded with the drug and MZF were investigated for growth inhibition of HepG2 cells under an AMF. The synergism of chemotherapy, magnetic hyperthermia, and the magnetothermally-facilitated drug release was also studied.

2. Experimental

2.1 Materials

The reagents, ϵ -caprolactone (CL), tin(II) 2-ethylhexanoate (Sn(Oct)₂), 3-(4,5-dimethyl-thiazol-2-yl)-2,5-diphenyltetrazolium bromide (MTT), 2-bromoisobutyryl bromide, triethylamine, 2-(2-methoxyethoxy)ethyl methacrylate (MEO₂MA), and oligo(ethylene glycol)methacrylate (OEGMA, $M_n = 475$) were obtained from Sigma-Aldrich. N,N,N',N',N'' -Pentamethyldiethylenetriamine (PMDETA) and dipentaerythritol were obtained from Acros Organics. A dialysis bag (molecular weight cut-off: 8000–14 000) was ordered from Sinopharm Chemical Reagent. Fetal bovine serum (FBS) was purchased from Hyclone. Trypsin-EDTA, penicillin-streptomycin, and high-glucose Dulbecco's modified Eagle's medium (DMEM) were purchased from Gibco.

CL was purified with CaH₂ for 48 h at room temperature and distilled under reduced pressure before use. Sn(Oct)₂ was distilled under reduced pressure. MEO₂MA and OEGMA were passed through a column of activated basic alumina to remove inhibitors. Dipentaerythritol was dried *in vacuo* at 60 °C for 24 h before use. Cuprous bromide (CuBr) was purified *via* stirring in acetic acid and washing with ethanol and then dried in a vacuum. 2-Bromoisobutyryl bromide was used without further purification.

2.2 Polymer synthesis and characterization

2.2.1 Synthesis of 6sPCL. Star-shaped poly(ϵ -caprolactone) (6sPCL) was synthesized by ring-opening polymerization (ROP) of CL using dipentaerythritol as an initiator and Sn(Oct)₂ as a catalyst. Typically, CL (41.09 g, 360 mmol), dipentaerythritol (0.60 g, 2.36 mmol) and a catalytic amount of Sn(Oct)₂ were added to a flame-dried polymerization tube. Argon gas was flushed through the tube three times until it was sealed.

Under magnetic stirring, polymerization was carried out at 115 °C for 24 h under an argon atmosphere. The crude polymer was dissolved in dichloromethane and precipitated in cold methanol three times. The purified 6-arm polymer was dried *in vacuo* until a constant weight was obtained.

$M_{n,NMR} = 17\,350$, $M_{n,GPC} = 15\,940$, $M_w/M_n = 1.19$. ¹H NMR (CDCl₃, δ , ppm): 4.06 (t, $-CH_2CH_2CH_2CH_2CH_2O$), 3.65 (t, $CH_2CH_2CH_2CH_2CH_2OH$), 2.31 (t, $CH_2CH_2CH_2CH_2CH_2O$), 1.65 (tt, $CH_2CH_2CH_2CH_2CH_2O$), 1.39 (tt, $CH_2CH_2CH_2CH_2CH_2O$).

2.2.2 Synthesis of 6sPCL-Br macroinitiator. 6sPCL was converted into an ATRP initiator by esterification of the $-OH$ group with 2-bromoisobutyryl bromide. In a typical example, 6sPCL (10 g, 3.46 mmol of hydroxyl groups) was dissolved in dichloromethane (50 mL) under stirring. Triethylamine (1.5 g, 14.82 mmol) was added to the solution under argon protection. The mixture was cooled to 0 °C under magnetic stirring. 2-Bromoisobutyryl bromide (2.382 g, 10.36 mmol) in dichloromethane (20 mL) was then added dropwise to the mixture within 40 min. The reaction mixture was stirred for 48 h under an argon atmosphere at room temperature. The filtrate was washed with dichloromethane and deionized water three times. The organic layer was concentrated on a rotary evaporator and precipitated in cold methanol three times. The resulting product was dried *in vacuo* at room temperature.

$M_{n,NMR} = 18\,140$, $M_{n,GPC} = 16\,750$, $M_w/M_n = 1.18$. ¹H NMR (CDCl₃, δ , ppm): 4.06 (t, $-CH_2CH_2CH_2CH_2CH_2O$), 2.30 (t, $CH_2CH_2CH_2CH_2CH_2O$), 1.93 (s, $C(CH_3)_2Br$), 1.65 (tt, $CH_2CH_2CH_2CH_2CH_2O$), 1.39 (tt, $CH_2CH_2CH_2CH_2CH_2O$).

2.2.3 Synthesis of 6sPCL-*b*-P(MEO₂MA-co-OEGMA) copolymers by ATRP. The 6sPCL-*b*-P(MEO₂MA-co-OEGMA) block copolymers were prepared by ATRP. In a typical procedure, PMDETA (68 mg, 0.39 mmol), CuBr (56 mg, 0.39 mmol), 6sPCL-Br macroinitiator (1.0 g, containing 0.33 mmol of C-Br groups), MEO₂MA (3.117 g, 16.56 mmol), OEGMA (0.684 g, 1.44 mmol) and THF (15 mL) were added in a dry Schlenk flask which was degassed with three freeze-evacuate-thaw cycles. MEO₂MA and OEGMA were added into the reaction flask by using a syringe under an argon atmosphere. Polymerization was performed at 50 °C for 5 h under magnetic stirring. The resulting product was dissolved in THF and passed through a basic alumina column to remove the copper catalysts. The polymer was obtained by precipitation into cold hexane and dried *in vacuo* at room temperature.

$M_{n,NMR} = 61\,270$, $M_{n,GPC} = 55\,720$, $M_w/M_n = 1.24$. ¹H NMR (CDCl₃, δ , ppm): 4.10–4.15 (t, $COOCH_2CH_2O$ in PMEO₂MA and POEGMA), 4.06 (t, $-CH_2CH_2CH_2CH_2CH_2O$ in PCL), 3.55–3.75 (t, $-CH_2CH_2O$ in PMEO₂MA and POEGMA), 3.32–3.45 (s, $-CH_2CH_2OCH_3$ in PMEO₂MA and POEGMA), 2.30 (t, $CH_2CH_2CH_2CH_2CH_2O$ in PCL), 1.95 (s, $-COC(CH_3)_2$), 1.85 (s, $-CH_2C(CH_3)-$ in PMEO₂MA and POEGMA), 1.65 (tt, $CH_2CH_2CH_2CH_2CH_2O$ in PCL), 1.38 (tt, $CH_2CH_2CH_2CH_2CH_2O$ in PCL), 0.88–1.04 (m, $-CH_2C(CH_3)-$ in PMEO₂MA and POEGMA).

2.3 Characterization methods

¹H NMR spectra were obtained with a Bruker DMX-500 ¹H NMR spectrometer with CDCl₃ as the solvent. The chemical

shifts for protons were determined with respect to tetramethylsilane (TMS) at $\delta = 0$ ppm. Attenuated total reflection Fourier transform infrared (FTIR) spectra were recorded on an AVATAR-360 ESP FTIR spectrometer. The average molecular weight and its distribution were determined using a gel permeation chromatographic (GPC) system equipped with a Waters 150C separations module and a Waters differential refractometer. The polymer samples were dissolved in THF at a concentration of 1–2 mg mL⁻¹. THF was eluted at 1.0 mL min⁻¹ through two Waters Styragel HT columns and a linear column. The morphology of copolymer micelles was studied using a transmission electron microscope (TEM, JEOL JEM-2010F, Japan) at an acceleration voltage of 120 kV. Briefly, a drop of micelles in a HEPES buffer solution was deposited on a copper grid. The sample was then stained with filtered phosphotungstic acid (PTA) before measurements.

2.4 Preparation and characterization of polymer micelles

2.4.1 Preparation and characterization of blank polymer micelles. Blank polymer micelles were prepared by dissolving the 6sPCL-*b*-P(MEO₂MA-*co*-OEGMA) copolymer in THF and adding into water within 30 min dropwise with magnetic stirring. The mixture was dialyzed against ultrapure water by using a dialysis membrane (molecular weight cut-off: 8000–14 000 g mol⁻¹) for 48 h. The water was refreshed every 6 h to remove the organic solvent. Finally the micellar solution was diluted into different concentrations with deionized water or a phosphate buffer solution (PBS, pH 7.4) for the following experiments. The size and the zeta potential of self-assembled micelles were determined at 25 °C by using a Nano-ZS 90 Nanosizer (Malvern Instruments, Worcestershire, UK). The critical micelle concentration (CMC) of the star-block copolymer was determined with pyrene as a hydrophobic fluorescent probe. The concentration of the copolymer varied from 3.9 × 10⁻³ mg mL⁻¹ to 0.2 mg mL⁻¹ and that of pyrene was fixed at 0.3 μM. Fluorescence spectra were recorded on a Hitachi F-2500 FL Spectrophotometer with the excitation wavelength of 334 nm. CMC was estimated by extrapolating the intensity of emission at 397 nm at low and high concentrations.

2.4.2 Preparation and characterization of self-assembled micelles encapsulated with the drug and MZF-MNPs. MZFs were prepared by the method of solution-phase thermal decomposition.^{24–26,33} Typical procedures of micelles encapsulated with the anti-tumor drug (DOX, doxorubicin) and MZF-MNPs (represented as DOX-MZF-micelles) are as follows. The 6sPCL-*b*-P(MEO₂MA-*co*-OEGMA) copolymer and DOX were dissolved in THF, followed by adding a MZF/THF dispersion into the solution. After ultrasonication for 15 min, the mixture was transferred into a dialysis bag (molecular weight cut-off: 8000–14 000 g mol⁻¹) and dialyzed against deionized water for 48 h. The water was refreshed every 6 h to remove the organic solvents. To remove unloaded MZF-MNPs, the solution was filtered through a 0.45 μm Millipore membrane filter. Finally, the remaining micellar solution was diluted to different concentrations with a phosphate buffer solution (PBS, pH 7.4). To determine the drug loading capacity, DOX-MZF-micelles were

lyophilized for 48 h and dissolved in THF. The DOX amount was quantified by UV absorption at 478 nm against a standard calibration curve. The drug loading content (DLC) was defined by the equation:

$$\text{DLC (\%)} = \left(\frac{\text{the mass of the drug loaded in micelles}}{\text{the mass of drug loaded micelles}} \right) \times 100\%$$

2.5 In vitro drug release behaviors

As a typical procedure, a 2.5 mL mixed micellar solution (1.0 mg mL⁻¹), encapsulated with the drug and MZF-MNPs in PBS (0.02 M, pH 7.4), was placed in a dialysis tube (cellulose membrane; MWCO is 3500 Da) and immersed into 250 mL PBS medium, magnetically stirred at 20 °C, 37 °C, and 43 °C, under an AMF ($f = 114$ kHz, $H_{\text{applied}} = 89.9$ kA m⁻¹). The DOX-MZF-micelles were treated with an AMF every 5 min per 24 h. Within 72 h, AMF was applied twice. Upon each sampling, a buffer solution of 5 mL was extracted from the dialysis tube outside and replaced with an equal volume of fresh PBS periodically. The drug concentration was then quantified by UV/Vis spectrophotometry and the cumulative release was calculated.

2.6 In vitro cytotoxicity assays

In vitro cytotoxicity of micelles against HepG2 cells was evaluated by the MTT assay. HepG2 cells were cultured in DMEM (containing 10% FBS) at 37 °C for 48 h. HepG2 cells were seeded on 96-well plates at 2.0 × 10³ cell density and incubated for 24 h. After DMEM was replaced with fresh medium, the cells were treated with varying concentrations of the pure micelles, MZF-micelles, DOX-micelles, and DOX-MZF-micelles. Meanwhile the cells were treated with free DOX (5 μg mL⁻¹) as the control. After incubating at 37 °C with 5% CO₂ for 48 h, the cells were washed with PBS and incubated for another 6 h. 20 μL PBS with the MTT reagent (5 mg mL⁻¹) was subsequently added into each well and the cells were incubated for another 4 h. The cell media were replaced with DMSO. The optical densities (OD) were evaluated by using a microtiter plate reader (BIO-RAD, USA) at 490 nm. The cell viability was calculated by the equation:

$$\text{Cell viability} = \left(\frac{\text{the OD value of a sample}}{\text{the OD value of the control}} \right) \times 100\%$$

The average half maximal inhibitory concentration (IC₅₀) values of the DOX-MZF-micelles at different time intervals were determined based on the MTT results.

The HepG2 cells were seeded in a culture dish (35 mm). Anti-tumor efficiencies of DOX-MZF-micelles under different conditions were evaluated by MTT, in which the DOX concentrations varied from 10⁻³ μg mL⁻¹ to 10 μg mL⁻¹. Upon exposure to 43 °C and an AMF ($f = 114$ kHz, $H_{\text{applied}} = 89.9$ kA m⁻¹, 5 min per 24 h), the cells were cultured in an incubator at 37 °C for 24 h. After incubating, cell survival was assessed by MTT quantitatively. Each sample was reduplicated four times.

The cellular uptake experiments were performed by using confocal laser scanning microscopy (CLSM). The HepG2 cells were seeded at 1.0 × 10⁵ cells per dish (35 mm) in 2.0 mL of DMEM (containing 10% FBS) at 37 °C for 24 h, and incubated

for an additional 24 h with DOX-MZF-micelles. During this period, the cells were incubated at 37 °C, and exposed to 43 °C (5 min per 24 h) under an AMF ($f = 114$ kHz, $H_{\text{applied}} = 89.9$ kA m^{-1} , treated 5 min per 24 h) respectively. The HepG2 cells were subsequently fixed with paraformaldehyde (4%) for 30 min in an incubator and the cell nuclei were stained with a DAPI solution. The fluorescence images of HepG2 cells were obtained by confocal laser scanning microscopy (CLSM, TCS SP, Leica, Germany).

3. Results and discussion

3.1 Synthesis and characterization of 6sPCL-*b*-P(MEO₂MA-co-OEGMA) copolymers

A group of 6sPCL-*b*-P(MEO₂MA-co-OEGMA) copolymers was obtained by the combination of living ring-opening polymerization (ROP) and atom transfer radical polymerization (ATRP) as depicted in Scheme 1. ¹H NMR characterization of the 6sPCL is presented in Fig. 1A. The peak of methylene protons (d) is detected at δ 4.06 ppm, as well as the other peaks as indicated in this figure (a-c). Terminal methylene protons (d') are found at δ 3.65 ppm. 6sPCL-Br macroinitiators were prepared by coupling excess 2-bromoisobutyryl bromide with the terminal hydroxyl groups of 6sPCL. The molecular weight of 6sPCL-Br increased slightly and the molecular weight distribution was similar to that of 6sPCL. As shown in Fig. 1B, the ¹H NMR spectrum of 6sPCL-Br indicates a new peak (e) at δ 1.93 ppm (methyl protons of 2-bromoisobutyryl bromide) and the complete disappearance of the peak at δ 3.65 ppm. These results indicate complete reactions of all terminal hydroxyl

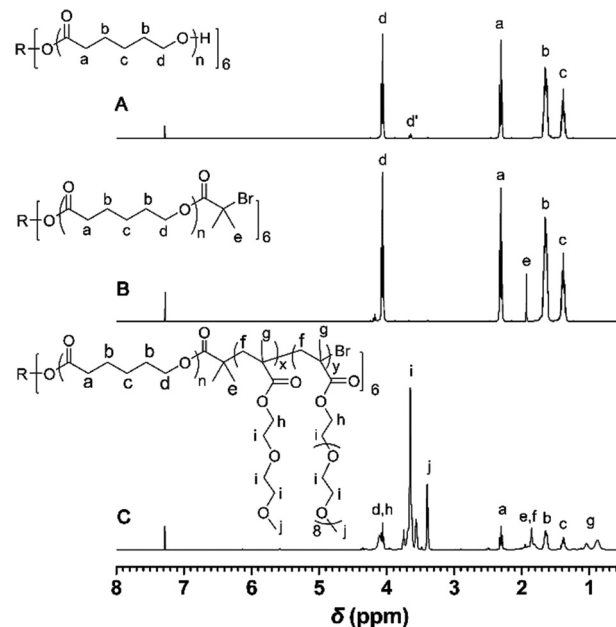
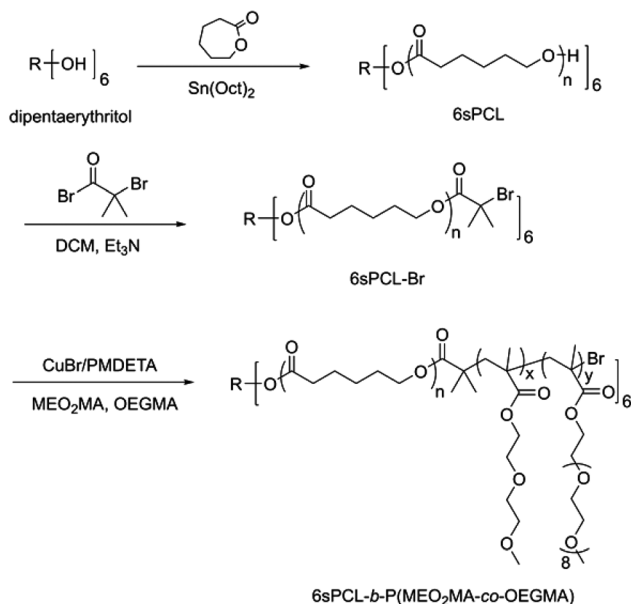


Fig. 1 ¹H NMR spectra of (A) star-shaped polymer 6sPCL, (B) star-shaped macroinitiator 6sPCL-Br, and (C) star-block copolymer 6sPCL-*b*-P(MEO₂MA-co-OEGMA).

groups of 6sPCL. 6sPCL-*b*-P(MEO₂MA-co-OEGMA) was prepared by ATRP of MEO₂MA and OEGMA co-monomers.

The feed molar ratio of MEO₂MA to OEGMA is 92/8. ¹H NMR spectra of these block copolymers show all the proton signals, consistent with their expected chemical structures (Fig. 1C). The peaks of methylene protons in PMEO₂MA and POEGMA (f, h, i) are also detected. Methyl protons (g) appear at δ 0.88–1.04 ppm. GPC analysis further supports the successful preparation of the co-polymers (Fig. 2). The GPC trace of 6sPCL-*b*-P(MEO₂MA-co-OEGMA) indicates its monomodal and symmetric characteristics. Compared with 6sPCL and



Scheme 1 Synthesis of star block copolymers by ring-opening polymerization (ROP) and atom transfer radical polymerization (ATRP).

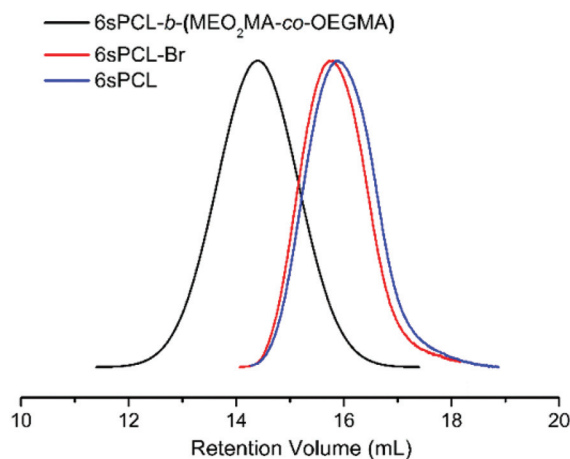


Fig. 2 GPC traces of 6sPCL, 6sPCL-Br and 6sPCL-*b*-P(MEO₂MA-co-OEGMA).

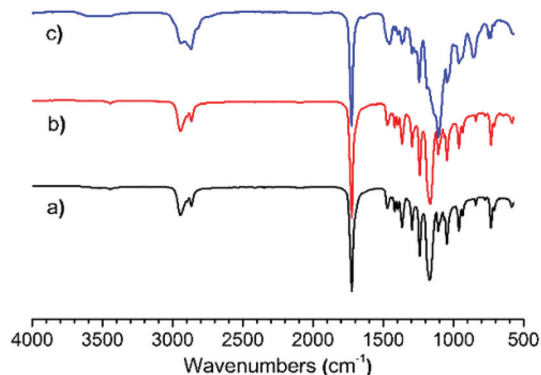


Fig. 3 FTIR spectra of (a) 6sPCL, (b) 6sPCL-Br, and (c) 6sPCL-*b*-P(MEO₂MA-*co*-OEGMA).

6sPCL-Br, the elution peak of 6sPCL-*b*-P(MEO₂MA-*co*-OEGMA) is shifted to a higher molecular weight as shown in Fig. 2.

FTIR spectra of the synthesized star-shaped polymers are shown in Fig. 3. The peak at 3360–3580 cm⁻¹ is the absorption band of the hydroxyl group and that at 1721 cm⁻¹ is assigned to the absorption peak of the ester bond of PCL segments. From Fig. 3c, it can be seen that the relative intensities of the carbonyl bond absorptions at 1723 cm⁻¹ are stronger than those of 6sPCL and 6sPCL-Br. Moreover, a new absorption peak at 1100 cm⁻¹ appears in Fig. 3c, indicating the presence of the C–O–C bonds which exist in the MEO₂MA-OEGMA copolymer. The new peak proves the successful introduction of MEO₂MA and OEGMA. These results well characterize the structure of the 6sPCL-*b*-P(MEO₂MA-*co*-OEGMA) block copolymer.

3.2 Self-assembly behavior of 6sPCL-*b*-P(MEO₂MA-*co*-OEGMA)

As shown in Fig. 4a, the MZF product was mainly monodisperse spherical nanocrystals with a relatively uniform diameter of 8 nm. The element ratio of Mn, Zn and Fe for MZF nanoparticles is 0.61/0.39/2 by inductively coupled plasma atomic emission spectroscopy (ICP-AES). With the hydrophobic PCL and hydrophilic P(MEO₂MA-*co*-OEGMA) blocks, 6sPCL-*b*-P(MEO₂MA-*co*-OEGMA) copolymers can spontaneously self-assemble into nanoscale micelles in PBS. The mixed micelles containing the drug and MZF-MNPs can be established by encapsulating hydrophobic DOX and MZF-MNPs into micellar cores physically. The blank polymer-, MZF-, and DOX-MZF-micelles prepared by a dialysis method were characterized by TEM, DLS, and fluorescence techniques. Typically, all these micelles exhibit a spherical morphology (Fig. 4). The apparent radius of 6sPCL-*b*-P(MEO₂MA-*co*-OEGMA) micelles observed by TEM is 115 nm (Fig. 4b). Under a TEM, it is clear that MZF-MNPs are encapsulated by the polymer. As a consequence, the diameter of MZF-micelles increases to 180 nm (Fig. 4c). Encapsulation of a hydrophobic drug results in further enlargement of DOX-MZF-micelles to 190 nm as shown in Fig. 4d.

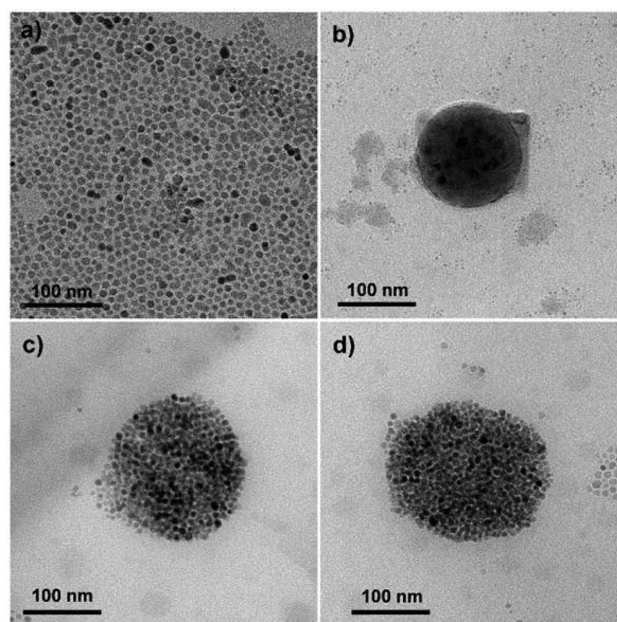


Fig. 4 TEM images of (a) the magnetic MZF nanoparticles, (b) blank 6sPCL-*b*-P(MEO₂MA-*co*-OEGMA) micelles, (c) MZF-micelles, and (d) DOX-MZF-micelles.

The formation of micelles from the star-block copolymers was verified by a fluorescence probe technique using pyrene. As shown in Fig. 5, the fluorescence intensity is approximately constant for a copolymer concentration of 47.7 mg L⁻¹. The intensity increases dramatically thereafter, indicating the formation of micelles and the transfer of pyrene molecules into the hydrophobic cores of the micelles. This concentration is defined as the critical micelle concentration (CMC). As shown in Fig. 5B, the 6sPCL-*b*-P(MEO₂MA-*co*-OEGMA) micelles exhibit the lowest CMC value of 47.7 mg L⁻¹.

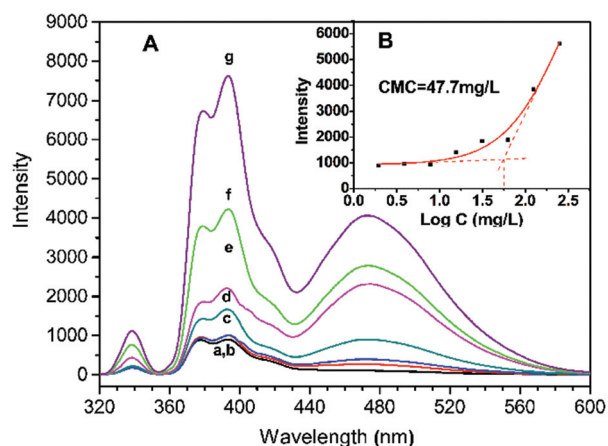


Fig. 5 Excitation spectra of pyrene in PBS at different concentrations of star-block copolymer micelles (A), and the critical micelle concentrations (CMC) of star-block copolymer micelles (B).

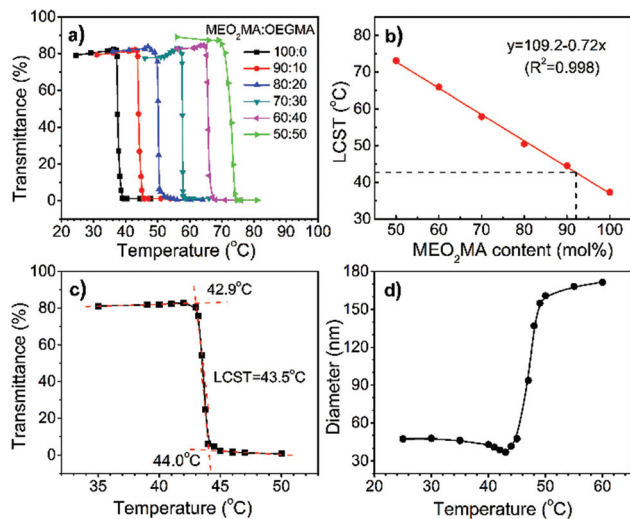


Fig. 6 (a) Transmittance curves and (b) plots of LCST as a function of MEO₂MA content for 6sPCL-*b*-P(MEO₂MA-*co*-OEGMA); (c) transmittance curves of 6sPCL-*b*-P(MEO₂MA92%-*co*-OEGMA8%) micelles, and (d) the diameter change of micelles in response to temperature.

3.3 Thermal phase transition properties of 6sPCL-*b*-P(MEO₂MA-*co*-OEGMA)

The synthesized copolymer 6sPCL-*b*-P(MEO₂MA-*co*-OEGMA) was assembled into nanoscale micelles in PBS. These micelles were formed from copolymers with different monomer feed ratios of MEO₂MA to OEGMA (50 : 50, 60 : 40, 70 : 30, 80 : 20, 90 : 10, 100 : 0). As shown in Fig. 6a and b, LCSTs of the copolymer micelles in PBS are dependent on the compositions of MEO₂MA and OEGMA. With the increase of the MEO₂MA ratio, the LCST of micelles decreased linearly from 73.1 °C to 37.3 °C. In this way, LCST can be well predicted as shown in Fig. 6b. For example, a well-defined copolymer 6sPCL-*b*-P(MEO₂MA-*co*-OEGMA) with a LCST of 43 °C is to be synthesized from an initial monomer feed of 92% of MEO₂MA. The LCST of the 6sPCL-*b*-P(MEO₂MA92%-*co*-OEGMA8%) copolymer micelles (Fig. 6c) is found to be close to the calculated value (Fig. 6b). The hydrodynamic diameters (D_h) and size changes of 6sPCL-*b*-P(MEO₂MA92%-*co*-OEGMA8%) micelles in aqueous solution were measured by DLS at different temperatures (Fig. 6d). When the temperature is below the LCST, the D_h values are small and change slightly. In contrast, the D_h values increase in the higher temperature range.

3.4 *In vitro* drug release behaviour of DOX-MZF-micelles

The thermo-responsive properties of the 6sPCL-*b*-P(MEO₂MA-*co*-OEGMA) micelles can be used for drug release control. Doxorubicin (DOX) was used as the model drug to investigate the drug release behavior by thermo-responses of the micelles in PBS at pH 7.4. The drug loading content (DLC) of DOX-MZF-micelles was finally calculated to be 5.0% according to the method in section 2.4.2. As shown in Fig. 7, significant changes in drug release near LCST of the copolymer are

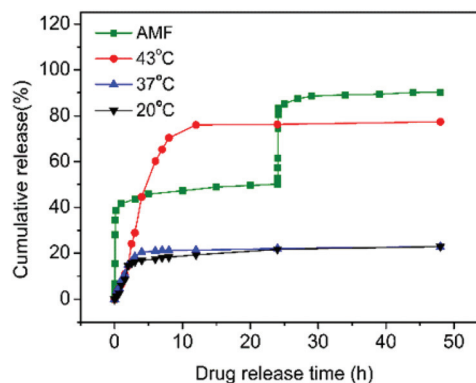


Fig. 7 *In vitro* cumulative DOX release profiles from DOX-MZF-micelles at 20 °C, 37 °C, and 43 °C under an AMF (treated for 5 min per 24 h).

observed. At 25 °C, a highly hydrated P(MEO₂MA-*co*-OEGMA) segment stabilizes the hydrophobic-hydrophilic core-shell structure of the copolymer micelles. Only a small amount of the drug is found to diffuse outwardly from the micelles. The drug release is rather slow at this temperature, and 78% drug still remains in the micelles after 48 h. However, the micelles exhibit a higher release rate when the temperature is raised to 43 °C. The P(MEO₂MA-*co*-OEGMA) chains located on the shell of micelles become hydrophobic and the core-shell structure is deformed. The hydrophobic DOX incorporated into the core is diffused out quickly and more than 70% drug is released from the micelles. The release rate of the model drug DOX can be effectively controlled by changing the external temperatures. Due to the unique magnetic heating properties of DOX-MZF-micelles, the drug release by AMF is even more rapid than the conditions at 43 °C. As shown in Fig. 7, the cumulative DOX release of DOX-MZF-micelles reaches 35% rapidly in 5 min. Without an AMF, drug release of micelles slows down in the next 24 h. When an AMF is re-applied, the cumulative DOX release increased over 80%. Therefore, an AMF can effectively raise the temperature of micelles within a short time, leading to a faster thermal phase transition of micelles and more significant drug release.

3.5 The cytotoxicity of DOX under different treatments

The cytotoxicities of the blank-, MZF-, DOX- and DOX-MZF-micelles were investigated by the MTT assay and CLSM. As shown in Fig. 8, the cell survival rates approximate 90% at the polymer concentrations ranging from 10 to 1000 $\mu\text{g mL}^{-1}$, indicating excellent biocompatibilities of the polymer- and MZF-micelles in HepG2 cells. Furthermore, the DOX- and DOX-MZF-micelles exhibit good inhibitory effects on the HepG2 cells at a low concentration (Fig. 9).

To investigate the anti-tumor effects on the micelles under chemotherapy, thermo-chemotherapy, and magnetic thermo-chemotherapy, the DOX-MZF-micelles were incubated with HepG2 cells at 37 °C as the chemotherapy control group, 43 °C (5 min per 24 h) as the thermo-chemotherapy group, and AMF treatment (5 min per 24 h) as the magnetic hyperthermia-

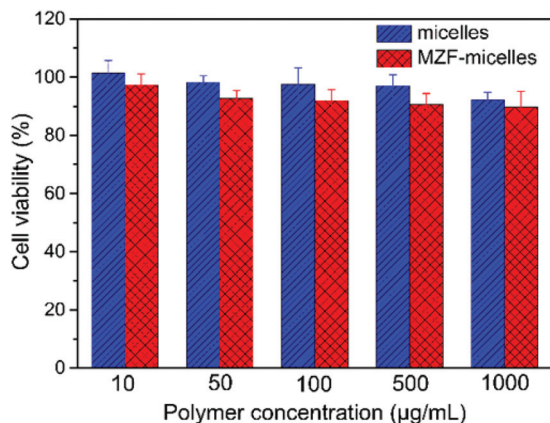


Fig. 8 Cytotoxicity of pure thermo-responsive micelles and MZF-micelles in HepG2 cells.

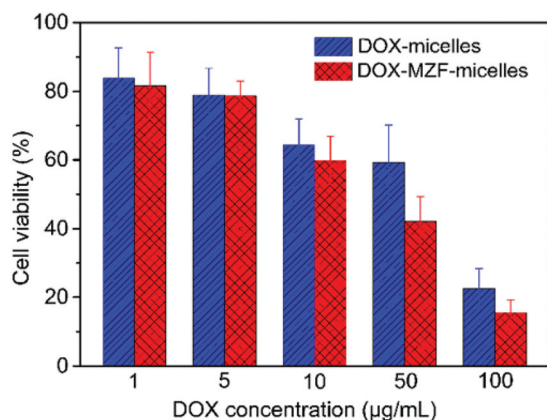


Fig. 9 Cytotoxicity of DOX-micelles and DOX-MZF-micelles in HepG2 cells.

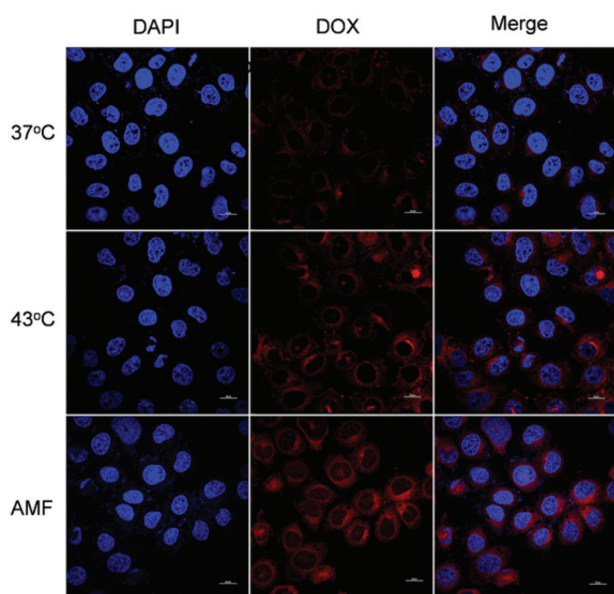


Fig. 10 CLSM images of MZF-DOX-micelles in HepG2 cells.

chemotherapy group for 24 h, 48 h and 72 h, respectively. The IC_{50} value (the concentration that inhibited cell growth by 50%) was calculated simultaneously. At 37 °C for 24 h, the IC_{50} value of DOX-MZF-micelles was as high as $6.228 \mu\text{g mL}^{-1}$. After raising the temperature to 43 °C, it decreased to $2.029 \mu\text{g mL}^{-1}$, which was nearly one-third of that at 37 °C. The notable reduction was mainly ascribed to the accelerated release of DOX. When the temperature reached the LCST of the drug-loaded micelles, the phase transformation of thermo-responsive micelles took place leading to more pronounced drug release. High uptake of DOX is clearly observed in the CLSM images (Fig. 10), showing the enhancement of anti-tumor efficiencies *via* hyperthermia. When treated with a periodic AMF (5 min per 24 h), the IC_{50} value of DOX-MZF-micelles dra-

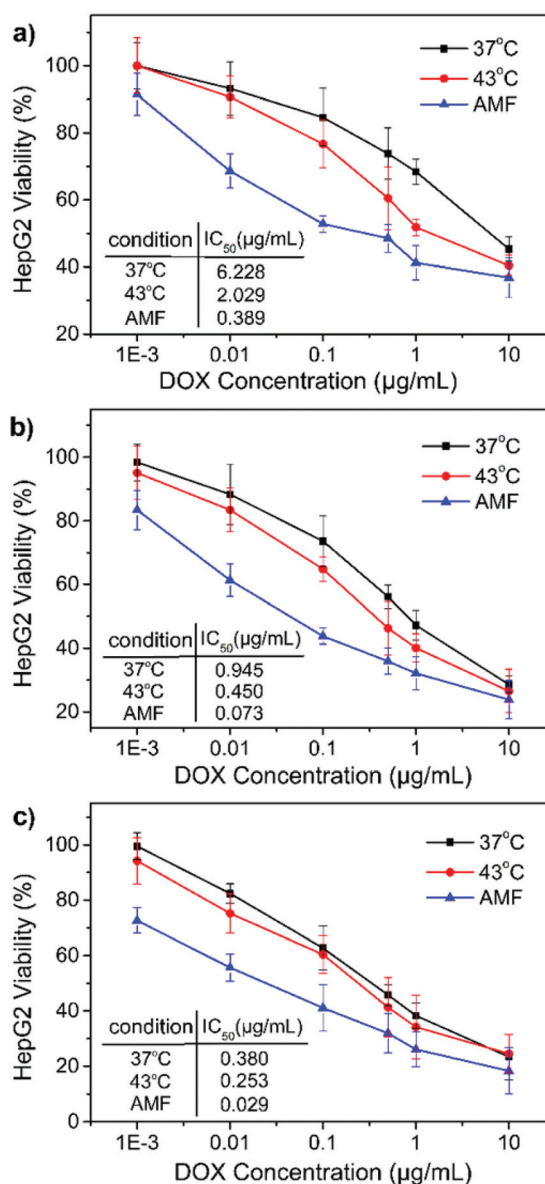


Fig. 11 Viability of HepG2 cells after treatment with DOX-MZF-micelles at different concentrations for 24 h (a), 48 h (b) and 72 h (c).

matically decreased to $0.389 \mu\text{g mL}^{-1}$, indicating that the cytotoxicity of DOX-MZF-micelles markedly enhanced by AMF.

MZF-MNPs are able to rapidly raise the temperature of micelles above LCST owing to their unique temperature responsive properties under an AMF even at low concentrations. The physical encapsulation of MZF-MNPs in the DOX-MZF-micelles has also improved the heating efficiency of micelles in HepG2 cells. Comparing the IC_{50} values under three different conditions for 24 h, 48 h and 72 h, the coefficients of synergism between the magnetic thermo-chemotherapy (under an AMF) and chemotherapy (at $43 \text{ }^\circ\text{C}$) are 5.22, 6.16 and 8.72, respectively. Furthermore, the synergism with increasing time can be seen in Fig. 11, as a result of drug accumulation. The MTT and CLSM results clearly show the advantages of combining magnetic hyperthermia with magnetothermally-facilitated drug release, which leads to significant synergism of chemotherapy and hyperthermia.

4. Conclusions

In conclusion, we have synthesized the star-block copolymer 6sPCL-P(MEO₂MA-co-OEGMA)s with different molar ratios of MEO₂MA to OEGMA. The amphiphilic star copolymers have self-assembled to form nanoscale micelles with a CMC of $47.7 \mu\text{g mL}^{-1}$. The LCST of the thermo-responsive micelles is well controlled at $43.5 \text{ }^\circ\text{C}$ by adjusting the content of MEO₂MA. The hydrophobic DOX and MZF-MNPs are efficiently encapsulated into micelles that facilitate *in vitro* DOX release from DOX-MZF-micelles at the temperature above LCST. The DOX-MZF-micelles show enhanced growth inhibition on HepG2 cells under an AMF. These magnetothermally responsive star-block copolymeric micelles can potentially be used in efficient drug delivery and effective thermo-chemotherapy.

Acknowledgements

The authors acknowledge the financial support from the National High Technology Research and Development Program of China (863 Program: no. 2013AA032202), the National Natural Science Foundation of China (no. 51203118), the Fundamental Research Funds for the Central Universities, and the Open Funds for Characterization of Tongji University.

Notes and references

- D. Sutton, N. Nasongkla, E. Blanco and J. Gao, *Pharm. Res.*, 2007, **24**, 1029–1046.
- S. M. Janib, A. S. Moses and J. A. MacKay, *Adv. Drug Delivery Rev.*, 2010, **62**, 1052–1063.
- R. Duncan, *Nat. Rev. Drug Discovery*, 2003, **2**, 347–360.
- G. A. Hussein and W. G. Pitt, *Adv. Drug Delivery Rev.*, 2008, **60**, 1137–1152.
- K. Hayashi, M. Nakamura, W. Sakamoto, T. Yogo, H. Miki, S. Ozaki, M. Abe, T. Matsumoto and K. Ishimura, *Theranostics*, 2013, **3**, 366–376.
- Y. Qu, J. B. Li, J. Ren, J. Z. Leng, C. Lin and D. L. Shi, *Nanoscale*, 2014, **6**, 12408–12413.
- Y. Qu, J. B. Li, J. Ren, J. Z. Leng, C. Lin and D. L. Shi, *ACS Appl. Mater. Interfaces*, 2014, **6**, 16867–16879.
- T. Kalland and I. Dahlquist, *Cancer Res.*, 1983, **43**, 1842–1846.
- B. Frey, E. M. Weiss, Y. Rubner, R. Wunderlich, O. J. Ott, R. Sauer, R. Fietkau and U. S. Gaipl, *Int. J. Hyperthermia*, 2012, **28**, 528–542.
- T. S. Hauck, T. L. Jennings, T. Yatsenko, J. C. Kumaradas and W. C. W. Chan, *Adv. Mater.*, 2008, **20**, 3832–3838.
- R. D. Issels, *Eur. J. Cancer*, 2008, **44**, 2546–2554.
- P. Schildkopf, O. J. Ott, B. Frey, M. Wadepohl, R. Sauer, R. Fietkau and U. S. Gaipl, *Curr. Med. Chem.*, 2010, **17**, 3045–3057.
- J. B. Li, J. Z. Leng, Y. Qu, L. Deng and J. Ren, *Mater. Lett.*, 2014, **131**, 5–8.
- Y. Qu, J. B. Li and J. Ren, *Prog. Chem.*, 2013, **25**, 785–798.
- H. Oliveira, E. Pérez-Andrés, J. Thevenot, O. Sandre, E. Berra and S. Lecommandoux, *J. Controlled Release*, 2013, **169**, 165–170.
- T. Todd, Z. Zhen, W. Tang, H. Chen, G. Wang, Y.-J. Chuang, K. Deaton, Z. Pan and J. Xie, *Nanoscale*, 2014, **6**, 2073–2076.
- Y. Liu, J. B. Li, J. Ren, C. Lin and J. Z. Leng, *Mater. Lett.*, 2014, **127**, 8–11.
- J. F. Lutz, Z. Akdemir and A. Hoth, *J. Am. Chem. Soc.*, 2006, **128**, 13046–13047.
- J. B. Li, J. Ren, Y. Cao and W. Z. Yuan, *Polymer*, 2010, **51**, 1301–1310.
- J. Ding, L. Zhao, D. Li, C. Xiao, X. Zhuang and X. Chen, *Polym. Chem.*, 2013, **4**, 3345–3356.
- W. Yuan, J. Zhang, J. Wei, H. Yuan and J. Ren, *J. Polym. Sci., Part A: Polym. Chem.*, 2011, **49**, 4071–4080.
- K. Hayashi, M. Nakamura, W. Sakamoto, T. Yogo, H. Miki, S. Ozaki, M. Abe, T. Matsumoto and K. Ishimura, *Theranostics*, 2013, **3**, 366–376.
- M. M. Yallapu, S. F. Othman, E. T. Curtis, B. K. Gupta, M. Jaggi and S. C. Chauhan, *Biomaterials*, 2011, **32**, 1890–1905.
- K. Cheng, S. Peng, C. J. Xu and S. H. Sun, *J. Am. Chem. Soc.*, 2009, **131**, 10637–10644.
- J. Lu, S. Ma, J. Sun, C. Xia, C. Liu, Z. Wang, X. Zhao, F. Gao, Q. Gong, B. Song, X. Shuai, H. Ai and Z. Gu, *Biomaterials*, 2009, **30**, 2919–2928.
- N. R. Jana, Y. Chen and X. Peng, *Chem. Mater.*, 2004, **16**, 3931–3935.
- M. Zheng, C. Yue, Y. Ma, P. Gong, P. Zhao, C. Zheng, Z. Sheng, P. Zhang, Z. Wang and L. Cai, *ACS Nano*, 2013, **7**, 2056–2067.
- J. Huang, L. Wang, R. Lin, A. Y. Wang, L. Yang, M. Kuang, W. Qian and H. Mao, *ACS Appl. Mater. Interfaces*, 2013, **5**, 4632–4639.

- 29 Y. Cao, J. Ren, J. B. Li and Y. Liu, *Mater. Lett.*, 2010, **64**, 1570–1573.
- 30 J. Lee, Y. Huh, Y. Jun, J. Seo, J. Jang, H. Song, S. Kim, E. Cho, H. Yoon, J. Suh and J. Cheon, *Nat. Med.*, 2007, **13**, 95–99.
- 31 U. I. Tromsdorf, N. C. Bigall, M. G. Kaul, O. T. Bruns, M. S. Nikolic, B. Mollwitz, R. A. Sperling, R. Reimer, H. Hohenberg, W. J. Parak, S. Förster, U. Beisiegel, G. Adam and H. Weller, *Nano Lett.*, 2007, **8**, 2422–2427.
- 32 J. Jang, H. Nah, J. H. Lee, S. H. Moon, M. G. Kim and J. Cheon, *Angew. Chem., Int. Ed.*, 2009, **48**, 1234–1238.
- 33 S. Sun, H. Zeng, D. B. Robinson, S. Raoux, P. M. Rice, S. X. Wang and G. Li, *J. Am. Chem. Soc.*, 2004, **126**, 273–279.